PAPER

Supplementary material

Geometry-Driven Dimensional Crossover from Weak Localization to Superconducting Fluctuations in Nanostructured NbN Networks

Priyank Tripathi,[a,b] Debashree Nayak [c] , Mandeep Kaur[a,b], Sahil Verma[a,b], Kartik Senapati[c], Sudhir Husale[a,b*]

Table of Content:

S.No.	Film material	Substrate	Technique	Thickness (nm)	T_C (K)	References
1.	NbN	Sapphire	Reactive sputtering	500	15.2	[1]
				2.5	6.5	
2.	NbN	MgO	Reactive sputtering	>50	9.9-16.1	[2]
3.	NbN	MgO	Reactive sputtering	>50	2.7-16.8	[3]
4.	NbN	MgO	Reactive sputtering	>50	11.9	[4]
5.	NbN	MgO	PLD	100	16	[5]
6.	NbN	Sapphire	HTCVD	40	17	[6]
7.	NbN	AlN/Al_2O_3	PVD epitaxy	5	11	[7]
				50	15	
8.	NbN	AlN/Al_2O_3	PVD	5	11.2	[8]
				50	15.3	
9.	NbN	Si+AlN buffer	Reactive sputtering	5	9.9	[9]
				50	14.5	
10.	NbN	Si (Flexible)	Magnetron sputtering	10	8.3	[10]
				50	11.9	
				100	12.4	
11.	NbN	Si	Ion-assisted sputtering	100	13	[11]
12.	NbN	Si	DC Magnetron sputtering	100	16	[12]
13.	NbN	MgO	PLD	50	13.1	[13]
		Al_2O_3		50	15.2	
		Sapphire		50	16.6	
14.	NbN	Si	Ion beam sputtering	100	13	[14]
15.	NbN	Si	Reactive sputtering	200	12.8	[15]
16.	ε-NbN	Bulk sample	HPHT synthesis	Bulk polycrystalline	11.6	[16]
	δ-NbN				17.5	
17.	Nb_2N	Si_3N_4/Si	DC Magnetron sputtering + nitridation	16	0.73	[17]
				11	0.68	
				8	0.62	
18.	NbN	SiO_2	DC Magnetron sputtering	144	13.8	Present work
		SiN		144	14.55	

Table S1 : Compilation of reported superconducting transition temperatures (**Tc**) of NbN thin films as a function of film thickness from the literature. The table summarizes the film material, substrate, growth technique, thickness, and corresponding Tc values reported in previous studies. For consistency across different reports, Tc values correspond to the **zero-resistance transition temperature (T_{c0})** wherever available. The dataset spans a wide range of film thicknesses and deposition techniques including reactive sputtering, magnetron sputtering,

[a.] *Academy of Scientific and industrial Research (AcSIR), Ghaziabad-201002, India.*
[b.] *Council of Scientific and Industrial Research, National Physical Laboratory, Dr. K.S. Krishnan Marg, New Delhi – 110012, India.*
[c.] *School of Physical Sciences, National Institute of Science Education and Research (NISER) Bhubaneswar, An OCC of Homi Bhabha National Institute, Jatni-752050, Odisha, India.*
* *Correspondance Email : husalesc.nplindia@csir.res.in*

pulsed laser deposition (PLD), chemical vapor deposition, and ion-assisted sputtering. Data for Nb_2N and ε-NbN phases are also included for comparison with related niobium nitride systems. The final entry corresponds to the NbN film investigated in the present work.

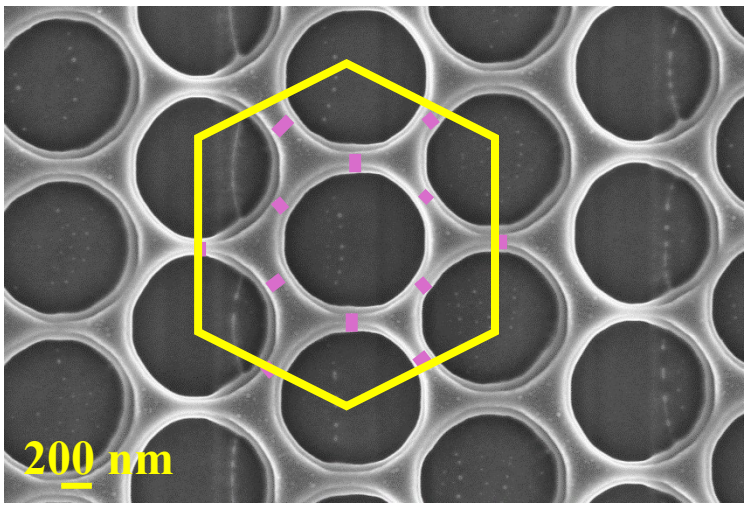

Supplementary Figure S1. FESEM image of NbN-NR3 device , Yellow hexagon is denoting the one unit cell and purple color lines are weak link spacing (s)

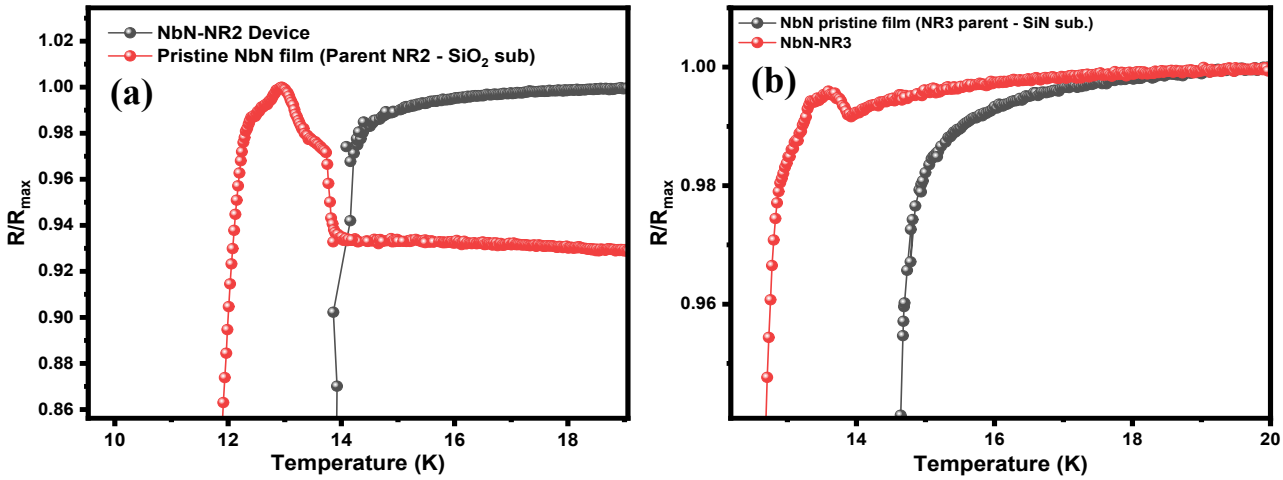

Supplementary Figure S2. Comparison between pristine and patterned NbN films. (a) R–T of the pristine NbN parent film for NbN-NR2 (144 nm, unpatterned): resistance decreases monotonically above Tc with no WL–SCF crossover. (b) R–T of the independently fabricated NbN-NR3 device (s ≈ 97.87 nm, SiN substrate) showing the same WL–SCF crossover as NR2, confirming that the crossover is geometry-driven and reproducible across devices on different substrates.

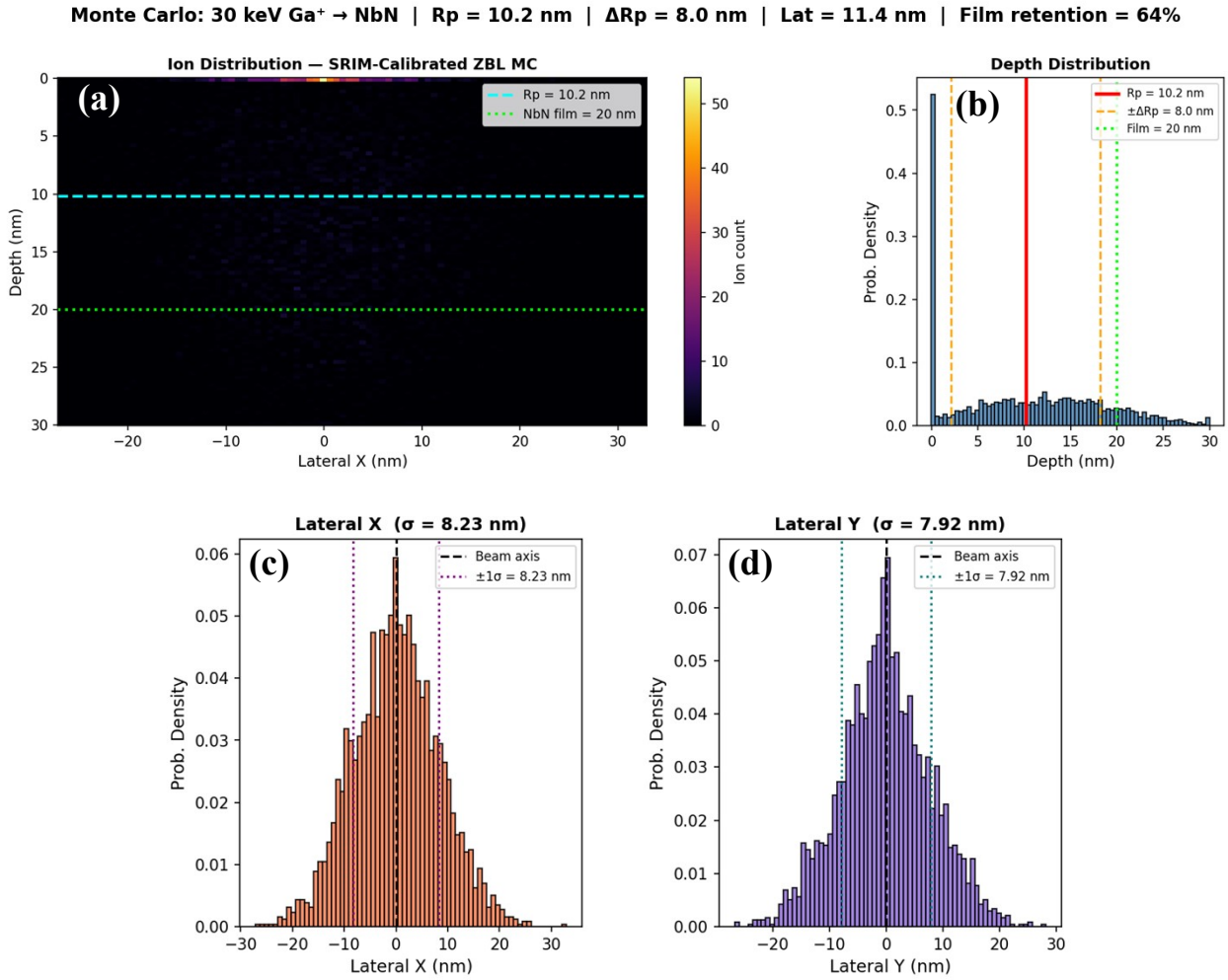

Supplementary Figure S3. SRIM/ZBL Monte Carlo simulations of Ga^+ ion damage in NbN (144 nm). (a) Ion range and lateral straggle distributions for 30 keV Ga^+ incident on NbN (b) . Depth profile of FIB milling. (d) Schematic cross-section showing undamaged NbN core (~35–52 nm) flanked by ~23 nm damaged edge zones on each side, consistent with projected range ~10 nm and lateral straggle ~8 nm.

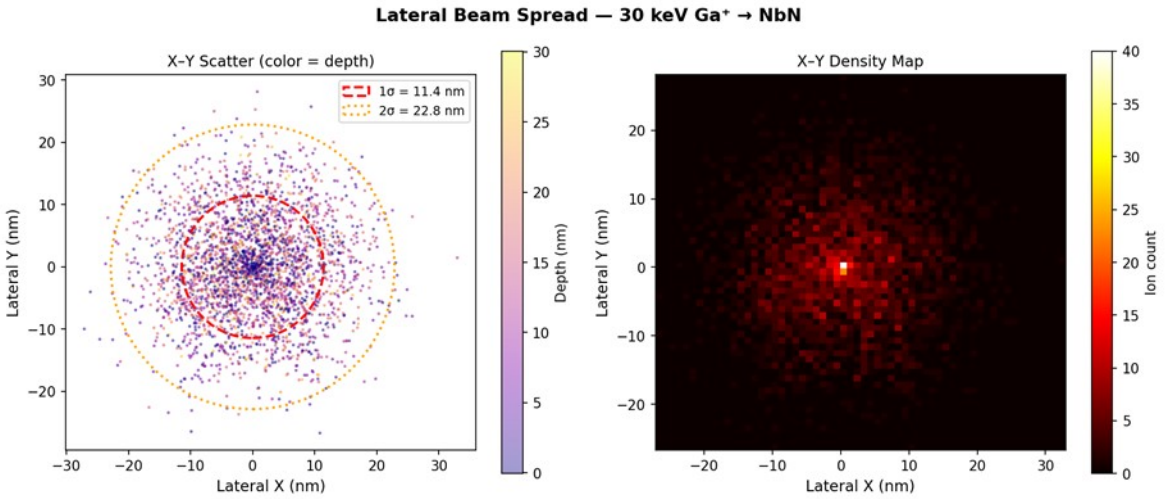

Supplementary Figure S4. Cross-section showing undamaged NbN core (~35–52 nm) flanked by ~23 nm damaged edge zones on each side . (a) 2D-scatter plot for showing the ion distribution around the hole edges. (b) 2D-ion density color map.

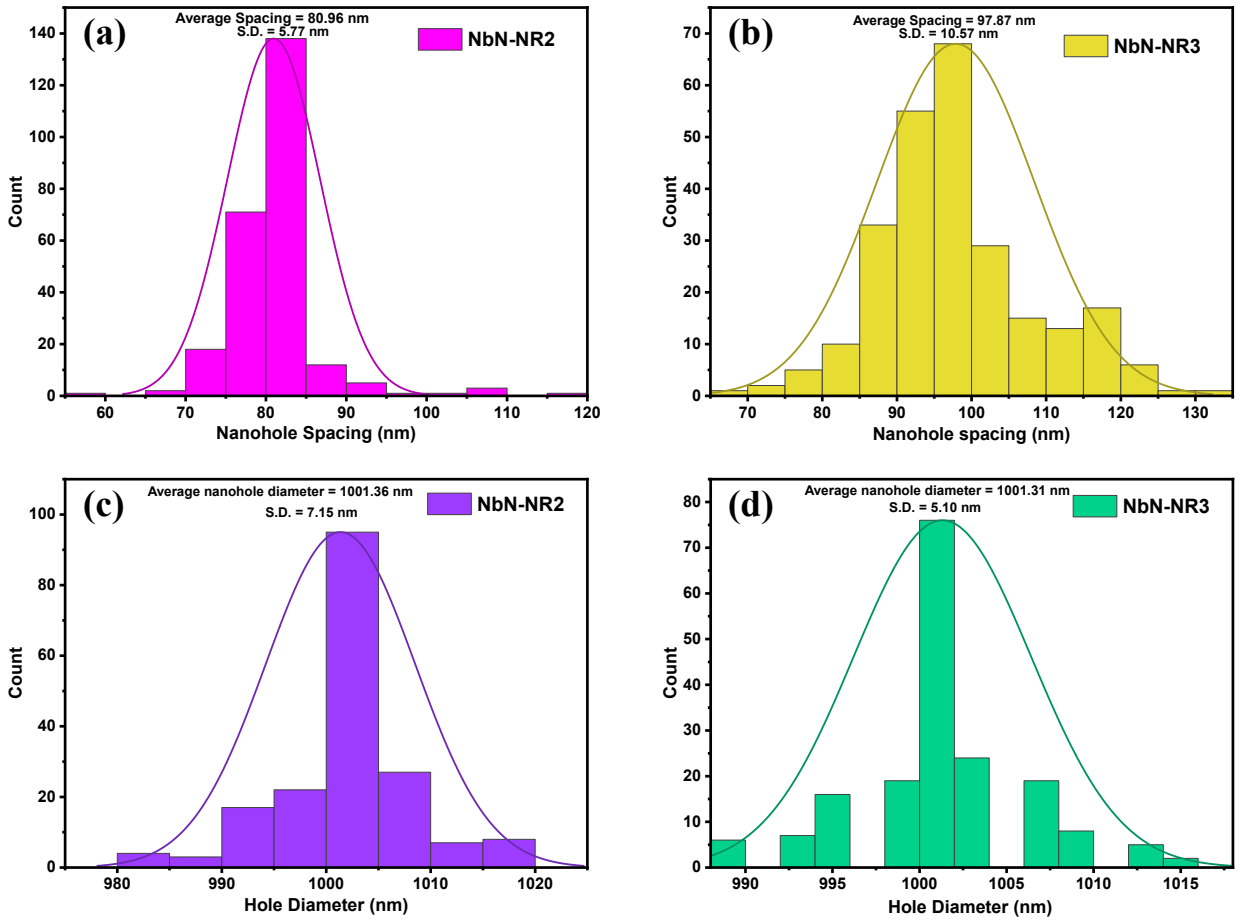

Supplementary Figure S5. Statistical characterization of FIB nanohole geometry. (a) Edge-to-edge spacing histogram for NR2 ~ 81 ± 6 nm, narrow Gaussian confirming uniformity. (b) Edge-to-edge spacing histogram for NR3 ~ 98 ± 10 nm. (c) Hole diameter histogram for NR2 ~1001 ± 7 nm. (d) Hole diameter histogram for NR3 ~1001 ± 5 nm. The narrow distributions demonstrate statistical uniformity of the FIB network; the resulting Tc variation of ~0.1–0.2 K is negligible compared to the multi-kelvin transport features observed.

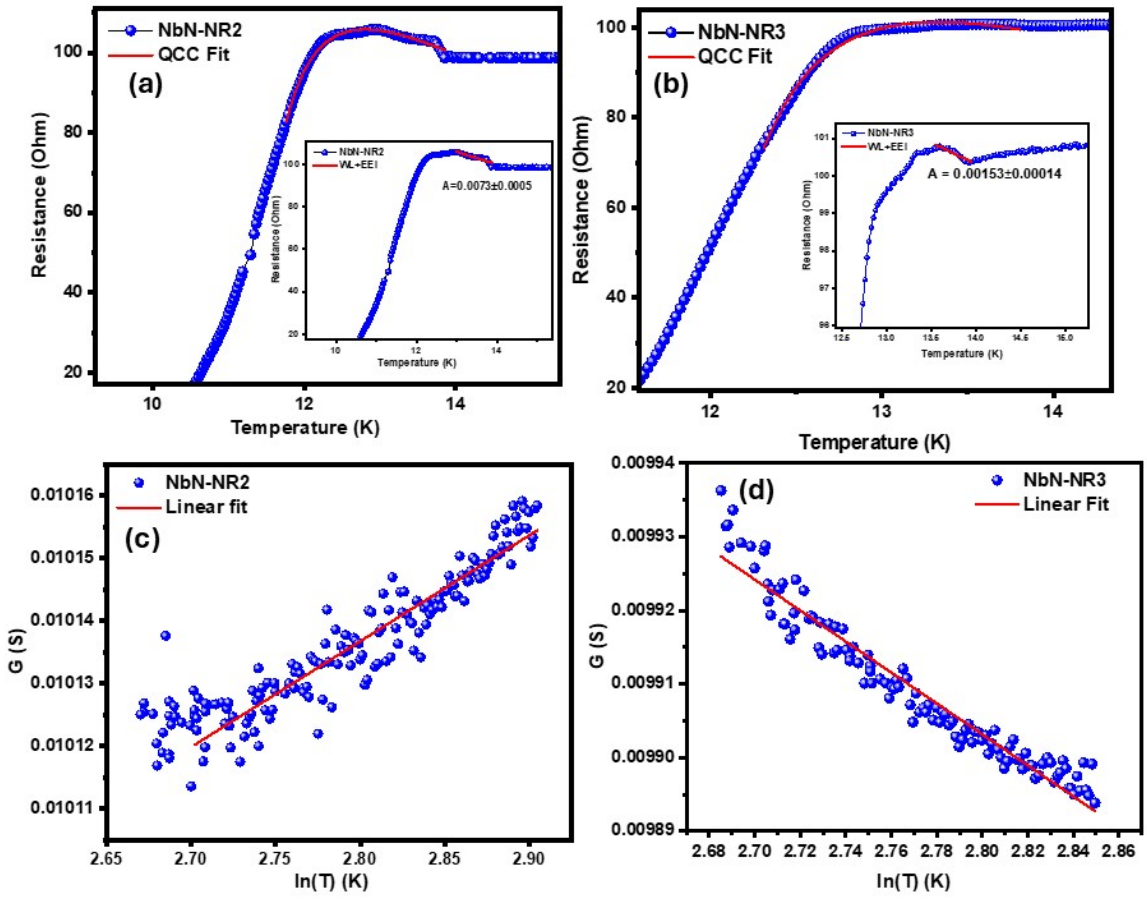

Supplementary Figure S6. QCC composite model fit. (a) QCC fit for NbN-NR2 inset is showing WL+EEI fit in resistance upturn region. (b) QCC fit for NbN-NR3 inset is showing WL+EEI fit in resistance upturn region. (c) G vs ln(T) for multi-kelvin temperature scale transport confirms long range competition of WL+SCF dominated 2D transport behavior for NbN-NR2. (d) G vs ln(T) for multi-kelvin temperature scale transport confirms competition of WL+SCF dominated 2D transport behavior for NbN-NR3.

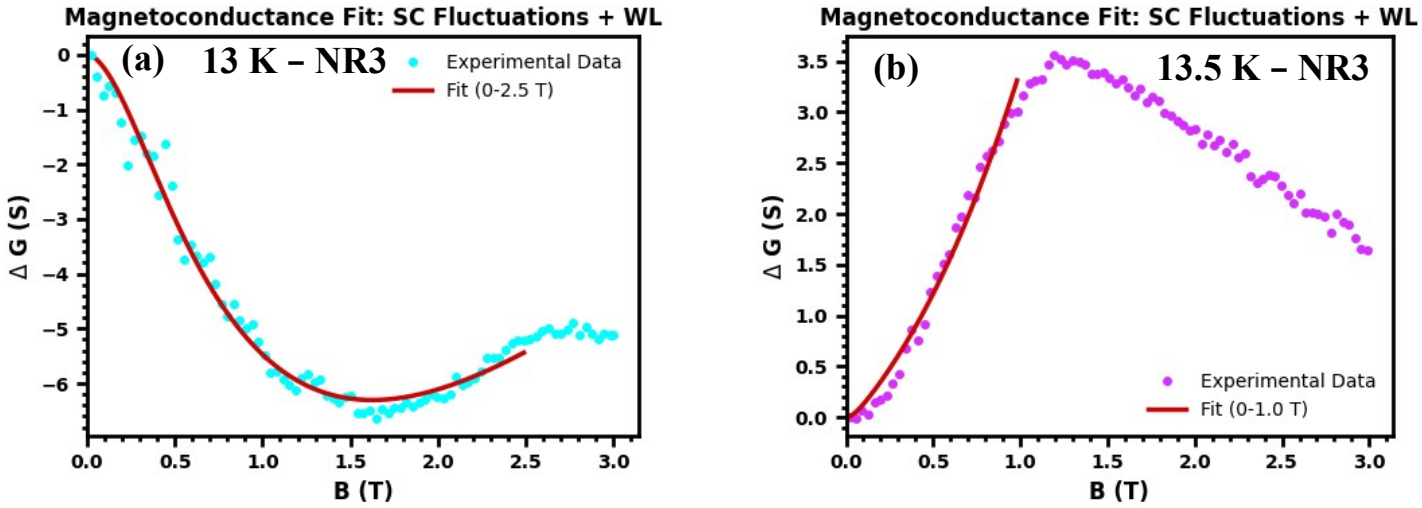

Supplementary Figure S7. Modified HLN magnetoconductance fitting for NbN-NR3 at T* = 13 K and Tpeak = 13.5 K. (a) ΔG vs. B at T = 13 K (crossover temperature T*): experimental data (cyan) and SCF+WL combined fit (red, 0–2.5 T). A clear conductance valley confirms simultaneous SCF and WL activity. Extracted: Bφ = 0.0175 T, BSF = 0.3839 T, lφ = 96.99 nm ≈ s = 97.87 nm, SCF/WL ratio = 1.054 (balanced — true crossover). (b) ΔG vs. B at T = 13.5 K (Tpeak): monotonically negative magnetoconductance (SCF-dominated, fit 0–1.05 T), no WL upturn. Extracted: Bφ = 0.0407 T, BSF = 2.384 T, lφ = 63.6 nm (lφ/s = 0.650 < 1, crossover not yet satisfied), SCF/WL = 0.917 (WL dominant).

T (K)	Bφ (T)	B_{SF} (T)	τ_{GL} (ps)	D (cm²/s)	τφ (ps)	lφ (nm)	l_T (nm)	ξ (nm)
13	0.0175	0.3839	2.612	1.642	57.295	96.99	24.63	3.87
13.5	0.0407	2.384	1.8415	0.375	107.87	63.6	11.55	1.84

Table S2. Characteristic parameters for NbN-NR3 at T^* = 13 K and T_{peak} = 13.5 K.

T (K)	C1 (AL)	C2 (MT)	C3 (WL)	C1+C2 (SCF)	SCF/WL ratio	Status
13	0.3851	0.1282	0.4866	0.5133	1.054	Balanced
13.5	0.0933	0.3945	0.5317	0.4878	0.917	WL dominant

Table S3. Relative coefficients for NbN-NR3 at T^* = 13 K and T_{peak} = 13.5 K.

Parameter	NbN-NR2	NbN-NR3
FIB spacing s (nm)	80.97	97.87
Bφ at crossover (mT)	21.35	17.50
lφ from Bφ (nm)	87.8	97.0
lφ / s	1.08	0.99
B_{SF} at crossover (mT)	230.9	383.9
l_T from B_{SF} (nm)	37.76	29.28

Table S4. Parameters extracted from modified HLN fitting at the WL–SCF crossover for NR2 and NR3.

Criterion	T = 13.5 K (T_{peak})	T = 13 K (T*)
lφ (nm)	63.6	96.99
lφ / s	0.650	0.991
SCF/WL ratio (C1+C2)/C3	0.917 (WL dominant)	1.054 (balanced)
B_{SF} (T)	2.384	0.384

Table S5. Four-criterion crossover diagnostic for NbN-NR3.

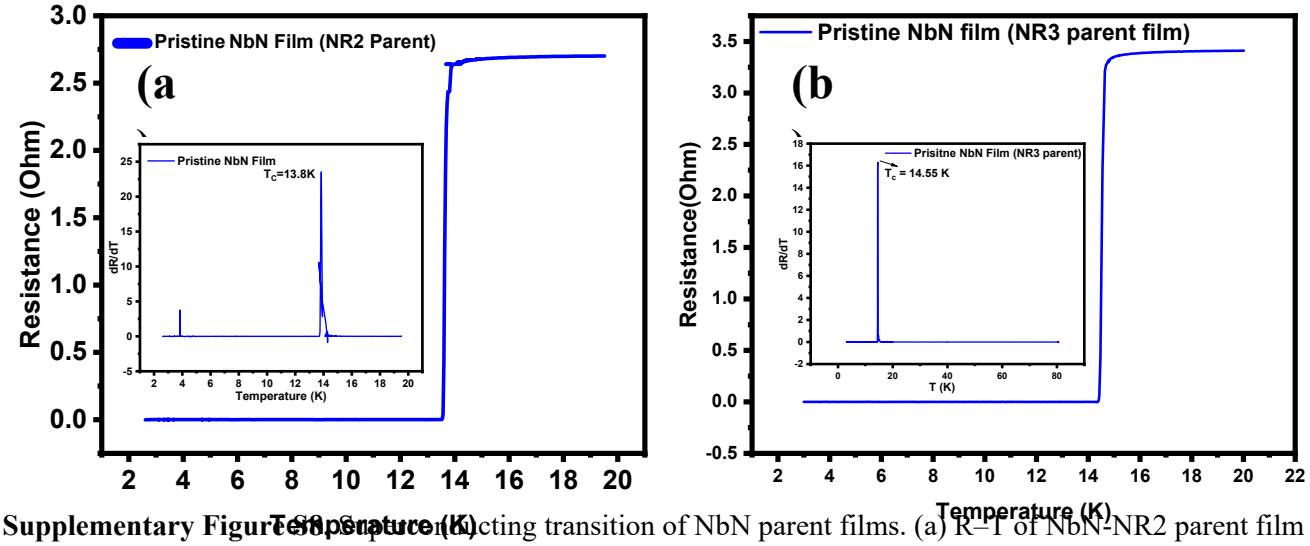

Supplementary Figure S8. Superconducting transition of NbN parent films. (a) R–T of NbN-NR2 parent film (144 nm, SiO_2): Tc = 13.8 K, exceeding the as-deposited benchmark of Ref. [12] (Tc ~ 11.8 K, same power, no annealing), confirming above-benchmark film quality. (b) R–T of NbN-NR3 parent film (144 nm, SiN): Tc = 14.55 K, surpassing the Chockalingam et al. power-matched value of 11.61 K at 40 W (Phys. Rev. B 77, 214503).

References

1. Gavaler, J.R., Janocko, M.A., Hulm, J.K. and Jones, C.K., 1971. Superconducting properties as a function of thickness in NbN films. *Physica*, *55*, pp.585-591.
2. Chockalingam, S.P., Chand, M., Jesudasan, J., Tripathi, V. and Raychaudhuri, P., 2008. Superconducting properties and Hall effect of epitaxial NbN thin films. *Physical Review B—Condensed Matter and Materials Physics*, *77*(21), p.214503.
3. Chand, M., Mishra, A., Xiong, Y.M., Kamlapure, A., Chockalingam, S.P., Jesudasan, J., Bagwe, V., Mondal, M., Adams, P.W., Tripathi, V. and Raychaudhuri, P., 2009. Temperature dependence of resistivity and Hall coefficient in strongly disordered NbN thin films. *Physical Review B—Condensed Matter and Materials Physics*, *80*(13), p.134514.
4. Chand, M., Saraswat, G., Kamlapure, A., Mondal, M., Kumar, S., Jesudasan, J., Bagwe, V., Benfatto, L., Tripathi, V. and Raychaudhuri, P., 2012. Phase diagram of the strongly disordered s-wave superconductor NbN close to the metal-insulator transition. *Physical Review B—Condensed Matter and Materials Physics*, *85*(1), p.014508.
5. Shapoval, T., Stopfel, H., Haindl, S., Engelmann, J., Inosov, D.S., Holzapfel, B., Neu, V. and Schultz, L., 2011. Quantitative assessment of pinning forces and magnetic penetration depth in NbN thin films from complementary magnetic force microscopy and transport measurements. *Physical Review B—Condensed Matter and Materials Physics*, *83*(21), p.214517.
6. Hazra, D., Tsavdaris, N., Jebari, S., Grimm, A., Blanchet, F., Mercier, F., Blanquet, E., Chapelier, C. and Hofheinz, M., 2016. Superconducting properties of very high quality NbN thin films grown by high temperature chemical vapor deposition. *Superconductor Science and Technology*, *29*(10), p.105011.
7. Wei, X., Roy, P., Yang, Z., Zhang, D., He, Z., Lu, P., Licata, O., Wang, H., Mazumder, B., Patibandla, N. and Cao, Y., 2021. Ultrathin epitaxial NbN superconducting films with high upper critical field grown at low temperature. *Materials Research Letters*, *9*(8), pp.336-342.
8. Licata, O.G., Sarker, J., Bachhav, M., Roy, P., Wei, X., Yang, Z., Patibandla, N., Zeng, H., Zhu, M., Jia, Q. and Mazumder, B., 2022. Correlation between thickness dependent nanoscale structural chemistry and superconducting properties of ultrathin epitaxial NbN films. *Materials Chemistry and Physics*, *282*, p.125962.
9. Yang, Z., Wei, X., Roy, P., Zhang, D., Lu, P., Dhole, S., Wang, H., Cucciniello, N., Patibandla, N., Chen, Z. and Zeng, H., 2023. CMOS-Compatible Ultrathin Superconducting NbN Thin Films Deposited by Reactive Ion Sputtering on 300 mm Si Wafer. *Materials*, *16*(23), p.7468.
10. Shi, H., Liang, L., Huang, Y., Bao, H., Jin, B., Wang, Z., Jia, X., Kang, L., Xu, W., Chen, J. and Wu, P., 2022. NbN films on flexible and thickness controllable dielectric substrates. *Scientific Reports*, *12*(1), p.10662.
11. Kosutova, T., Yao, Y., Fernandes, D., Zhang, Z., Zhang, S.L., Gustavo, F., Lefloch, F. and Kubart, T., 2025. Ion-assisted sputter-deposition of superconducting NbN thin films on silicon. *Superconductor Science and Technology*, *38*(9), p.095010.
12. Pei, Y., Fan, Q., Ni, X. and Gu, X., 2024. Controlling the Superconducting Critical Temperature and Resistance of NbN Films through Thin Film Deposition and Annealing. *Coatings*, *14*(4), p.496.
13. Volkov, S., Gregor, M., Roch, T., Satrapinskyy, L., Grančič, B., Fiantok, T. and Plecenik, A., 2019. Superconducting properties of very high quality NbN thin films grown by pulsed laser deposition. *Journal of Electrical Engineering*, *70*(7), pp.89-94.
14. Polakovic, T., Lendinez, S., Pearson, J.E., Hoffmann, A., Yefremenko, V., Chang, C.L., Armstrong, W., Hafidi, K., Karapetrov, G. and Novosad, V., 2018. Room temperature deposition of superconducting niobium nitride films by ion beam assisted sputtering. *APL materials*, *6*(7).
15. Kalal, S., Gupta, M. and Rawat, R., 2021. N concentration effects on structure and superconductivity of NbN thin films. *Journal of Alloys and Compounds*, *851*, p.155925.
16. Zou, Y., Qi, X., Zhang, C., Ma, S., Zhang, W., Li, Y., Chen, T., Wang, X., Chen, Z., Welch, D. and Zhu, P., 2016. Discovery of superconductivity in hard hexagonal ε-NbN. *Scientific reports*, *6*(1), p.22330.
17. Gajar, B., Yadav, S., Sawle, D., Maurya, K.K., Gupta, A., Aloysius, R.P. and Sahoo, S., 2019. Substrate mediated nitridation of niobium into superconducting Nb2N thin films for phase slip study. *Scientific reports*, *9*(1), p.8811.